Anisotropic polarization π-molecular skeleton coupled dynamics in proton-displacive organic ferroelectrics

J. Fujioka,[1] S. Horiuchi,[2] N. Kida,[1] R. Shimano,[1,3] and Y. Tokura[1,2,4,5]
[1]*Multiferroics Project, ERATO, Japan Science and Technology Agency, Wako 351-0198, Japan*
[2]*National Institute of Advanced Industrial Science and Technology (AIST), Tsukuba 305-8562, Japan*
[3]*Department of Physics, University of Tokyo, Tokyo 113-0033, Japan*
[4]*Department of Applied Physics, University of Tokyo, Tokyo 113-8656, Japan*
[5]*Cross-Correlated Materials Research Group (CMRG), RIKEN Advanced Science Institute, Wako 351-0198, Japan*
(Received 29 June 2009; revised manuscript received 25 August 2009; published 30 September 2009)

We have investigated the polarization π-molecular skeleton coupled dynamics for the proton-displacive organic ferroelectrics, cocrystal of phenazine with the 2,5-dihalo-3,6-dihydroxy-p-benzoquinones by measurements of the terahertz/infrared spectroscopy. In the course of the ferroelectric-to-paraelectric transition, the ferroelectric soft phonon mode originating from the intermolecular dynamical displacement is observed in the imaginary part of dielectric spectra ϵ_2, when the electric field of the light (E) is parallel to the spontaneous polarization (P). The soft phonon mode is isolated from the intramolecular vibrational mode and hence the intramolecular skeleton dynamics is almost decoupled from the polarization fluctuation. In the spectra for E parallel to the hydrogen-bonded supramolecular chain, by contrast, the vibrational mode mainly originating from the oxygen atom motion within the π-molecular plane is anomalously blurred and amalgamated into the polarization relaxation mode concomitantly with the dynamical proton disorder. This indicates that the dynamical disorder of the intramolecular skeleton structure, specifically that of oxygen atom, is strongly enhanced by the proton fluctuation and is significantly coupled to the polarization fluctuation along the hydrogen-bonded supramolecular chain. The results are discussed in terms of the proton-mediated anisotropic polarization π-molecular skeleton interaction, which characterizes these emerging proton-displacive ferroelectrics.

DOI: 10.1103/PhysRevB.80.125134 PACS number(s): 77.84.Jd, 78.30.Jw, 77.80.−e

I. INTRODUCTION

Ferroelectricity in organic materials has been extensively studied for these decades and is now of great renewed interest also in the light of emerging organic electronics.[1–4] In many of conventional organic ferroelectrics, the electric polarization is induced by the orientation or displacement of the polar constituent molecule. The prototypical example is a crystal of thiourea $(NH_2)_2C=S$ (Refs. 1 and 5) in which the ferroelectricity results from the collective rotation of the electric dipoles inherent in the polar constituent molecules. The manifestation of ferroelectricity is, however, accidental in many cases and hence there have been few useful guidelines for developing the organic ferroelectricity so far. Recently, a strategy for designing room-temperature organic ferroelectrics has been developed utilizing the intermolecular collective proton displacement.[3,6] In the developed materials, the interplay among proton, charge, and lattice degrees of freedom plays a crucial role in the emergence of the spontaneous polarization; the constituent molecules are interconnected with the hydrogen bond and the collective intermolecular proton displacement induces the electric polarization concomitantly with the asymmetric molecular distortion via the strong proton π-molecular skeleton interaction. In this paper, we report on the anomalous polarization π-molecular skeleton coupled dynamics in these proton-displacive molecular ferroelectrics, which may arise from the proton-mediated strong correlation between the polarization relaxation and the molecular skeleton shape dynamics.

The prototypical example for such materials is the cocrystal of phenazine (Phz) with the bromanilic acid (H_2ba), which exhibits a displacive-type ferroelectric transition.[6] We display the schematic view of the molecular structure for Phz-H_2ba in Fig. 1(a). Phz and H_2ba molecules alternately line up along the a axis and are interconnected with each other by the hydrogen bond, forming the one-dimensional hydrogen-bonded supramolecular chains. Each molecule is stacked with the π electron overlap in individual columns along the b axis. At room temperature, the system is paraelectric and both Phz and H_2ba molecules locate at the center of the inversion symmetry. As temperature (T) decreases, the paraelectric-to-ferroelectric transition occurs at $T_{C1}=138$ K and the spontaneous electric polarization (P) emerges along the b axis. At T_{C1}, both molecules relatively shift to each other as shown by arrows in Fig. 1(a). Kumai *et al.*[7] have shown that one of two protons for H_2ba molecule displaces toward the nitrogen atom of Phz molecule and the other remains almost unchanged, leading to the asymmetric molecular structure as shown in Fig. 1(b). The polarization reversal can be achieved by the collective proton displacement along the supramolecular chain. The possible two configurations of the asymmetric molecular structure are schematically shown in Fig. 1(b). Although such an asymmetric molecular structure induces the dipole moment along the supramolecular chain, the antiferroelectric interchain coupling cancels out the net polarization parallel to the a axis. With further decreasing T, sequential phase transitions occur at $T_{C2}=102$ K and $T_{C3}=99$ K.[8] It was revealed by the x-ray diffraction experiment that the incommensurate lattice modulation emerges in a narrow T interval between T_{C2} and T_{C3}, and the multiplication of the lattice structure with the threefold periodicity, that is, the periodic proton lattice, appears

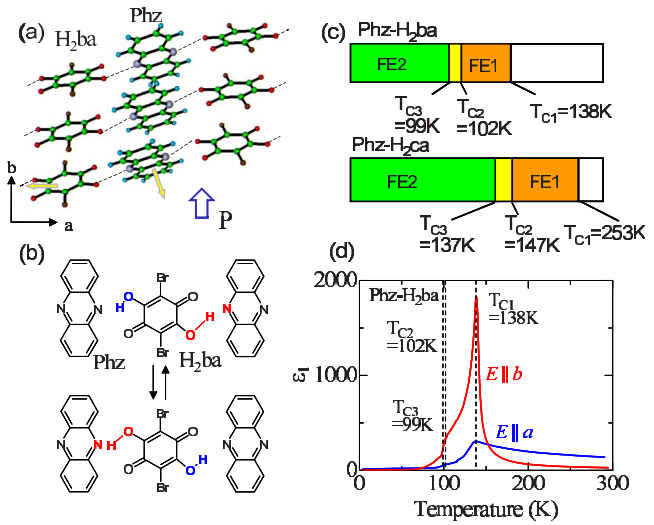

FIG. 1. (Color online) (a) Schematic view of the molecular structure in Phz-H_2ba. The dashed lines indicate the intermolecular hydrogen bond. The blue arrow indicates the spontaneous polarization. The yellow arrows indicate the molecular displacement related to the ferroelectric transition. (b) Schematic view of the intermolecular proton displacement in Phz-H_2ba. The blue (red) parts are the protonated (deprotonated) π-conjugated fragment corresponding to the enol form of the β diketone. Two possible configurations of the collective proton displacement are shown. (c) The dielectric phase diagram as a function of temperature for Phz-H_2ba (upper) and Phz-H_2ca (lower). (d) Temperature dependence of the real part of dielectric constant (measured at a frequency of 1MHz) for $E \| b$ (red line) and $E \| a$ (blue line). The vertical dashed lines indicate the phase-transition temperatures; $T_{C3}=99$ K, $T_{C2}=102$ K, and $T_{C1}=138$ K from left to right, respectively.

along the supramolecular chain below T_{C3}. These sequential phase transitions are schematically displayed in Fig. 1(c). The magnitude of polarization does not significantly change at T_{C2} and T_{C3}, and almost saturates at 1 $\mu C/cm^2$ below 50 K. We show the T dependence of the real part of dielectric constant measured at 1 MHz ($\epsilon_1^{1\ \mathrm{MHz}}$) in Fig. 1(d). At room temperature, $\epsilon_1^{1\ \mathrm{MHz}}$ with the electric field parallel to the b axis ($E \| b$) is as small as 30 while it exhibits a divergent behavior and reaches as large as 2000 around T_{C1} with decreasing T. With further decreasing T, it monotonically decreases and shows kinks at T_{C2} and T_{C3}. On the other hand, $\epsilon_1^{1\ \mathrm{MHz}}$ for $E \| a$ exceeds 100 at room temperature and shows a cusp at T_{C1}, reflecting that the dipole moment along the supramolecular chain is antiferroelectrically coupled along the c axis.[7] Similar anisotropic T dependence of the dielectric constant is observed also in the conventional hydrogen-bonded ferroelectrics such as KH_2PO_4 (KDP) (Ref. 9) in which the hydrogen-bond direction is also orthogonal to the spontaneous polarization direction. The ferroelectricity is appreciably stabilized by replacing H_2ba molecule with chloranilic acid (H_2ca) one. In Phz-H_2ca, the paraelectric-to-ferroelectric phase transition is identified at $T_{C1}=253$ K.[8,10,11] The incommensurate lattice modulation and the multiplication of the lattice structure with the two-fold periodicity emerge along the supramolecular chain at $T_{C2}=147$ K and $T_{C3}=137$ K, respectively, as schematically shown in Fig. 1(c). At the low-temperature phase, the saturated electric polarization is as large as 2 $\mu C/cm^2$, which is almost twice of that of Phz-H_2ba.

As already shown for the existing hydrogen-bonded dielectrics including both organic and inorganic materials, the proton-mediated polarization-lattice coupled dynamics plays a crucial role in the ferroelectric (or antiferroelectric) transition and the related dielectric anomaly.[12–15] In the present proton-displacive organic ferroelectrics, the highly anisotropic dielectric property as mentioned above may originate from the proton-mediated correlation between the polarization fluctuation and π-molecular skeleton dynamics, which should be explored by the low-frequency (far-infrared) and molecular-vibrational optical spectra. In this work, we have investigated the T dependence of the infrared optical spectra for Phz-H_2ba and Phz-H_2ca to reveal the polarization π-molecular skeleton dynamics coupled to the dynamical intermolecular proton displacement and discuss the origin of the dielectric anomalies. The present paper is organized as follows; In Sec. II, we describe the detailed experimental methods. Section III is devoted to the results and discussions. In Sec. III A, we present the results of the molecular vibration which is sensitive to the ionicity of the molecule and discuss the intermolecular dynamical proton displacement for both Phz-H_2ba and Phz-H_2ca. In Sec. III B, we describe the results of the dielectric spectra for $E \| b$ and discuss the relation between the polarization fluctuation and the molecular skeleton dynamics along the π-molecular stacking direction. In Sec. III C, we present the results of the dielectric spectra for $E \| a$. We discuss the proton-mediated strong correlation between the in-plane π-molecular skeleton dynamics and the polarization fluctuation along the supramolecular chain. Section IV is devoted to the conclusion.

II. EXPERIMENTAL METHODS

Single crystals of Phz-H_2ba and Phz-H_2ca were cocrystallized by the acetone diffusion method. The details of crystal growth have been reported elsewhere.[8] We have utilized the specular surface of these crystals as large as 3×3 mm^2 for optical measurements. The reflectivity spectra were recorded in the frequency range of 20–40 000 cm^{-1} from 10 K up to room temperature for both polarizations of the light E field; parallel to the π-molecular stacking direction (b axis) and to the hydrogen-bonded supramolecular chain (a axis). In the frequency range of 20–7000 cm^{-1}, we employed the Fourier transform infrared spectrometer. In the range of 4000–40 000 cm^{-1}, the reflectivity spectra were collected with the grating spectrometer. The real and imaginary parts of dielectric spectra (ϵ_1 and ϵ_2) were calculated by the Kramers-Kronig analysis. To obtain the $E \| b$ dielectric spectra for Phz-H_2ba in the frequency range of 10–40 cm^{-1}, we performed the terahertz (THz) time-domain spectroscopy with the transmittance geometry, which directly yields the complex dielectric spectra without resorting to the Kramers-Kronig analysis. The femtosecond laser pulses from the Ti:sapphire laser were irradiated to a ZnTe crystal, which leads to the generation of the THz waves. We utilized the dipole antenna coupled with the low-temperature-grown GaAs pho-

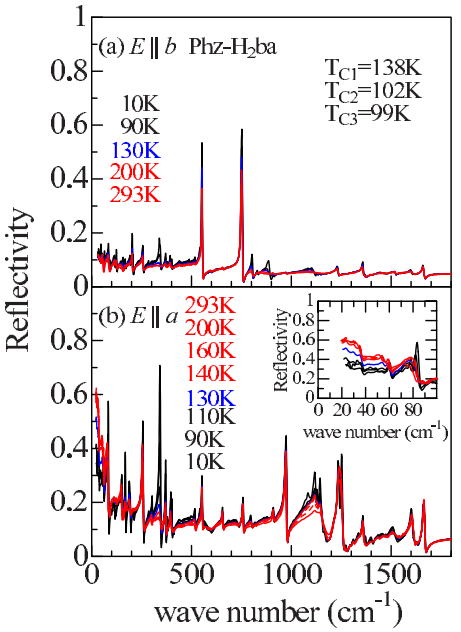

FIG. 2. (Color online) The reflectivity spectra of Phz-H_2ba at various temperatures for (a) $E\|b$ and (b) $E\|a$. The inset is the magnified view of the $E\|a$ reflectivity spectra below 100 cm^{-1}.

toconducting device to detect the THz waves. The details of the THz spectroscopy setup have been described elsewhere.[16]

III. RESULTS AND DISCUSSION

A. Dynamical proton disorder in the course of the periodic proton lattice melting

In Fig. 2(a), we show the T dependence of the $E\|b$ reflectivity spectra for Phz-H_2ba.

At 10 K, sharp peaks originating from the molecular vibrations are identified below 1700 cm^{-1}. Most of peaks show a minimal T dependence and are slightly blurred as T increases. In Fig. 2(b), we show the $E\|a$ reflectivity spectra at various temperatures. Many sharp peaks with a larger intensity are observed at 10 K. As T increases, several peaks are dramatically blurred and alternatively a high reflectance band reminiscent of the soft phonon mode shows up below 60 cm^{-1} as shown in the inset of Fig. 2(b). A similar behavior is observed for Phz-H_2ca (data not shown).

In Fig. 3(a), the imaginary part of $E\|a$ dielectric spectra (ϵ_2) for Phz-H_2ba is plotted in the frequency range of 1480–1720 cm^{-1}. Three peaks at 1560, 1610, and 1650 cm^{-1} are assigned to the monovalent C-O (C-O$^-$), C=C, and C=O stretching mode in H_2ba moiety, respectively.[8,18] Among them, the C-O$^-$ stretching mode can be used as a probe for the dynamical proton state since the intermolecular proton displacement enhances the intermolecular charge transfer or equivalently the ionicity of H_2ba molecule as pointed out by a recent theoretical study.[19] The appearance of the C-O$^-$ stretching mode at 10 K is consistent with the previously proposed picture that the periodic proton lattice with the quasi-ionic state is formed as the ground

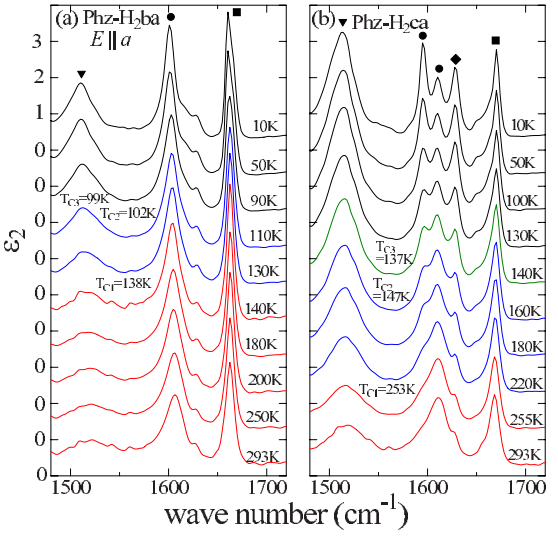

FIG. 3. (Color online) The imaginary part of the $E\|a$ dielectric spectra ϵ_2 at various temperatures in the frequency range of 1480–1720 cm^{-1} for (a) Phz-H_2ba and (b) Phz-H_2ca. The closed triangles, circles, and squares indicate the C-O$^-$ stretching mode, C=C stretching mode, and C=O stretching mode for H_2xa moiety, respectively. The closed diamonds indicate the C=C stretching mode for Phz moiety (Ref. 17).

state.[4] As T increases, the peak structure of the C-O$^-$ stretching mode is gradually blurred while that of the C=C and C=O stretching mode remains almost unchanged. To estimate the intermolecular charge fluctuation, or equivalently the dynamical proton displacement more quantitatively, we fitted the C-O$^-$ stretching mode with the Lorentz-type oscillator,

$$\epsilon_2(\omega) = \frac{S\omega_0^2\gamma\omega}{(\omega^2-\omega_0^2)^2+\omega_0^2\gamma^2} + \epsilon_2^{bg}.$$

Here, S is the oscillator strength, ω_0 the mode frequency, γ the damping rate, and ϵ_2^{bg} the contribution from the background mostly originating from the T-dependent tail of the neighboring modes. We estimated the spectral weight of the mode as $S\omega_0^2$ and plotted it as a function of T in Fig. 4(a). Below T_{C3} ($\sim T_{C2}$), the spectral weight shows minimal T dependence while it starts to decrease above T_{C3} ($\sim T_{C2}$) with increasing T. A recent structural study by Kumai *et al.*[7] has revealed that the thermal proton distribution is significantly broadened above T_{C2} while the molecular structure remains to be asymmetric up to T_{C1}. Thus, it is anticipated that the dynamical proton disorder accompanying the intermolecular charge fluctuation is enhanced in the course of the melting of the periodic proton lattice. It should be noted that the spectral weight is finite even above T_{C1}. This suggests that the molecules remain to be quasi-ionic on the time scale longer than the molecular vibration, that is, the dynamical proton disorder subsists even at the nominally neutral paraelectric phase.

In Fig. 3(b), we show the $E\|a$ ϵ_2 spectra for Phz-H_2ca in the frequency range of 1480–1720 cm^{-1}. The C-O$^-$ stretching mode is clearly identified at low temperatures while its

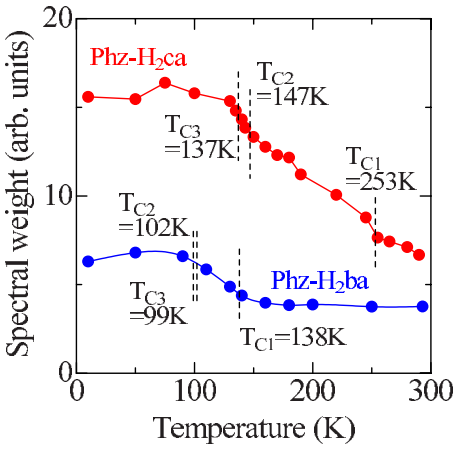

FIG. 4. (Color online) The temperature dependence of the spectral weight for the C-O$^-$ stretching mode (indicated by closed triangle in Fig. 3) of H_2ba moiety (blue line) and H_2ca one (red line). The vertical dashed lines indicate T_{C3}, T_{C2}, and T_{C1} from left to right.

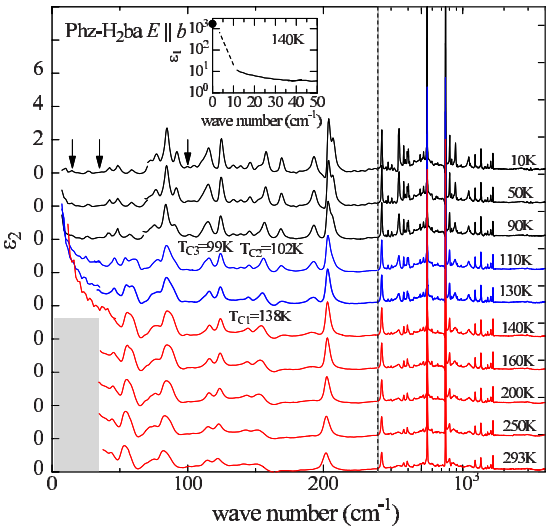

FIG. 5. (Color online) The imaginary part of the $E\|b$ dielectric spectra ϵ_2 for Phz-H_2ba in the frequency range of 0–4000 cm^{-1}. In the frequency range of 240–4000 cm^{-1}, the spectra are plotted on a logarithmic scale of wave number. The arrows indicate the frequency at 15, 35, and 100 cm^{-1} from left to right. The shaded area corresponds to the frequency range, where we cannot measure the transmission THz time-domain spectra because of large absorption (Ref. 20). The inset displays the real part of dielectric spectra ϵ_1 in the frequency range of 0–50 cm^{-1} at 140 K. The closed circle corresponds to ϵ_1(1 MHz) at 140 K.

peak shape is gradually blurred with increasing T as in the case of Phz-H_2ba. The spectral weight of the C-O$^-$ stretching mode is plotted as a function of T in comparison with that of Phz-H_2ba in Fig. 4. The overall T dependence of the spectral weight for this system is similar to that for Phz-H_2ba. It is evident that the spectral weight for Phz-H_2ca is more than twice of that for Phz-H_2ba at 10 K. This indicates that the magnitude of the proton displacement is larger in Phz-H_2ca than in Phz-H_2ba, which is consistent with the results of the recent neutron-diffraction measurement.[7,8] It should be noted that the C=C stretching mode for H_2ca moiety is split below T_{C1} as T decreases from room temperature. The splitting of the C=C stretching mode can be attributed to the nonequivalent two C=C bonds or equivalently to the asymmetric π-molecular skeleton distortion of H_2ca moiety in the ferroelectric phase; one of the two π-conjugated fragments corresponding to the enol form of the β diketone (HO-C=C-C=O) is slightly deprotonated by the intermolecular displacement and another remains to be protonated as shown in Fig. 1(b). Such a splitting of the C=C stretching mode is not appreciable for Phz-H_2ba in which the proton displacement is smaller than in Phz-H_2ca. This suggests that the magnitude of the asymmetric in-plane molecular skeleton distortion is closely tied with the intermolecular proton displacement via the proton π-molecular skeleton interaction. Since the molecular skeleton dynamics for Phz-H_2ca is similar to that for Phz-H_2ba, we focus on the result for Phz-H_2ba in the following sections.

B. Molecular skeleton dynamics along the π-molecular stacking direction

In this section, we present the results for the molecular skeleton dynamics along the π-molecular stacking direction, which is parallel to the spontaneous polarization (b axis) in Phz-H_2ba. In Fig. 5, we show the T dependence of the $E\|b$ ϵ_2 spectra. At 10 K, many sharp peak structures originating from the molecular vibrations and the translation/libration lattice modes are identified in the wide frequency range of 40–1700 cm^{-1}. The assignment of the representative peak structures is listed in Table I.[17,18] Since the molecular plane is almost perpendicular to the π-molecular stacking direction, the molecular vibrations which originate from the out-of-plane molecular deformation are predominantly observed. As T increases, the spectral weight below 30 cm^{-1} gradually increases and at 140 K ϵ_2 appears to be divergent in the limit of zero frequency.[20] Such a low-frequency optical excitation is extensively observed in a variety of ferroelectrics in the course of the ferroelectric-to-paraelectric transition and is assigned to the polarization relaxation or the soft phonon mode.[21] In the present system, the ferroelectric transition is displacive and accompanies the intermolecular displacement as displayed in Fig. 1(a).[6] Thus, the observed low-frequency

TABLE I. The assignment of the representative peak structures in the frequency range of 40–1700 cm^{-1} for the $E\|b$ spectrum at 10 K (Refs. 17 and 18).

Frequency (cm^{-1})	Assignment	Frequency (cm^{-1})	Assignment
53	Lattice mode	750	H_2baA_u
84	H_2baA_u	802	Phz B_{3u}
92	Phz B_{3u}	886	H_2baB_u
203	H_2ba	1111	Phz B_{1u}
256	H_2baA_u	1365	H_2baB_u
342	?	1649	H_2baB_u
551	H_2baA_u		

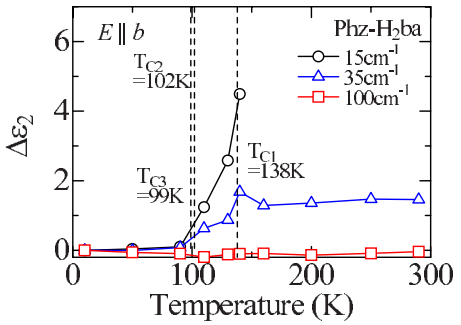

FIG. 6. (Color online) The temperature dependence of $\Delta\epsilon_2$ at 15 cm^{-1} (open circles), 35 cm^{-1} (open triangles), and 100 cm^{-1} (open squares) for Phz-H_2ba. Here, we defined $\Delta\epsilon_2=\epsilon_2(T)-\epsilon_2(10\ \mathrm{K})$ (see also text).

optical excitation may be interpreted as the soft phonon mode originating from the dynamical intermolecular displacement as displayed in Fig. 1(a). In the inset of Fig. 5, we show ϵ_1 spectra in the frequency range below 50 cm^{-1} as well as ϵ_1 (1 MHz) at 140 K. ϵ_1 at 10 cm^{-1} (~300 GHz) is still as small as 10 while ϵ_1 (1 MHz) is more than 1000. This suggests that the characteristic frequency of the soft phonon mode responsible for the dielectric anomaly near T_{C1} is much lower than 300 GHz. It should be noted that the tail of the soft phonon mode in ϵ_2 spectra appears to vanish at most around 50 cm^{-1}. To quantitatively appreciate this behavior, we identified the T dependence of the tail of the soft phonon mode at respective frequency as $\Delta\epsilon_2=\epsilon_2(T)-\epsilon_2(10\ \mathrm{K})$. In Fig. 6, we plotted the T dependence of $\Delta\epsilon_2$ at 15, 35, and 100 cm^{-1}. $\Delta\epsilon_2$ at 15 and 35 cm^{-1} exhibits a considerable T dependence while that at 100 cm^{-1} is almost T independent. This suggests that the soft phonon mode is almost decoupled from the molecular vibration modes lying at higher frequencies than 50 cm^{-1}. In other words, it is expected that the polarization fluctuation related to the ferroelectric transition predominantly originates from the dynamical intermolecular displacement and barely correlated with the out-of-plane intramolecular skeleton dynamics. This is perhaps because the proton displacement is not significantly coupled to the out-of-plane molecular distortion, which is contrastive with the case of the molecular dynamics along the supramolecular chain. The correlation between the proton dynamics and the fluctuation of the in-plane molecular skeleton structure is discussed in the next section.

C. Proton π-molecular skeleton dynamics along the supramolecular chain

In Fig. 7, we show the $E\|a$ ϵ_2 spectra for Phz-H_2ba in the frequency range of 0–100 cm^{-1} at various temperatures.[22] At 10 K, a few peak structures due to the librational/translational mode or the intramolecular vibrational mode can be identified. The assignment of the representative peak structures is listed in Table II.[17,18] Since the supramolecular chain is almost parallel to the π-molecular plane of each moiety, most of the intramolecular vibrations originate from the in-plane molecular skeleton dynamics. As T increases, these peaks are gradually blurred and alternatively a broad

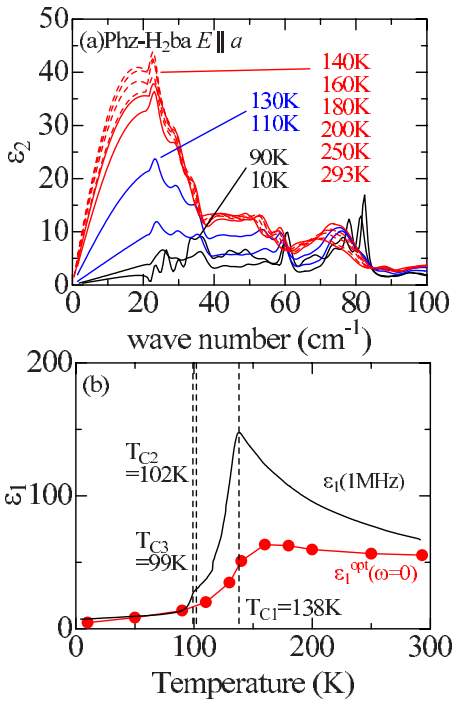

FIG. 7. (Color online) (a) The imaginary part of the $E\|a$ dielectric spectra ϵ_2 at various temperatures in the frequency range of 0–100 cm^{-1} for Phz-H_2ba. (b) The temperature dependence of ϵ_1(1 MHz) (solid line) and $\epsilon_1^{opt}(\omega=0)$ (closed circles). Here, $\epsilon_1^{opt}(\omega=0)$ is defined as the extrapolated value of ϵ_1 spectra to $\omega\to 0$ (see also text). The vertical dashed lines indicate T_{C3}, T_{C2}, and T_{C1} from left to right.

hump structure emerges around 20 cm^{-1}. In general, such a low-frequency optical excitation is closely related to the dielectric anomaly in the audio-frequency range. In Fig. 7(b), we plot the extrapolated value of ϵ_1 to $\omega\to 0$ ($\epsilon_1^{opt}(\omega=0)$) as well as ϵ_1(1 MHz) as a function of T. At 10 K, $\epsilon_1^{opt}(\omega=0)$ is less than 5, which is comparable to ϵ_1(1 MHz). As T increases, $\epsilon_1^{opt}(\omega=0)$ steeply increases above T_{C2} (~T_{C3}) and then slightly decreases above T_{C1}. Such a T dependency is qualitatively consistent with that of ϵ_1(1 MHz) while a large discrepancy between the two values is identified around T_{C1}.[23] It is clear that the broad hump structure around 20 cm^{-1} contributes to the dielectric anomaly in the audio-

TABLE II. The assignment of the representative peak structures in the frequency range of 40–1700 cm^{-1} for the $E\|a$ spectrum at 10 K (Refs. 17 and 18).

Frequency (cm^{-1})	Assignment	Frequency (cm^{-1})	Assignment
61	Lattice mode	550	H_2baB_u
78	Lattice mode	972	H_2baB_u
82	Lattice mode	1115	Phz B_{1u}
150	H_2baB_u	1235	H_2baB_u
254	Phz B_{1u}	1512	H_2baB_u
338	H_2baB_u	1605	H_2baB_u
370	H_2baB_u	1665	H_2baB_u

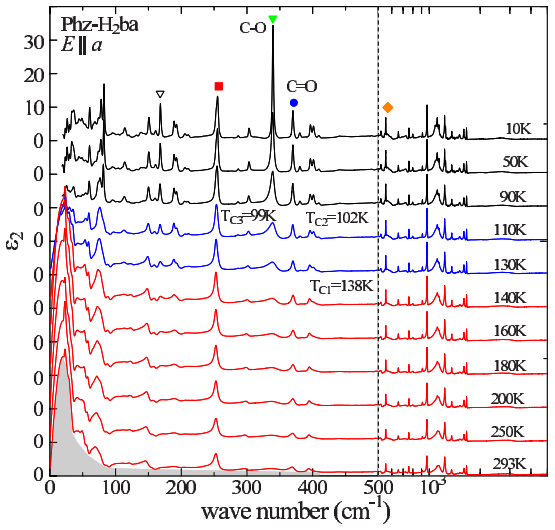

FIG. 8. (Color online) The $E\|a$ ϵ_2 spectra for Phz-H_2ba in the frequency range of 0–5000 cm^{-1} at various temperatures. The shaded area indicates the polarization relaxation mode at 293 K to guide the eyes. The marked molecular vibration modes are argued in the text and Fig. 9. Above 500 cm^{-1}, the abscissa for the frequency is described on a logarithmic scale.

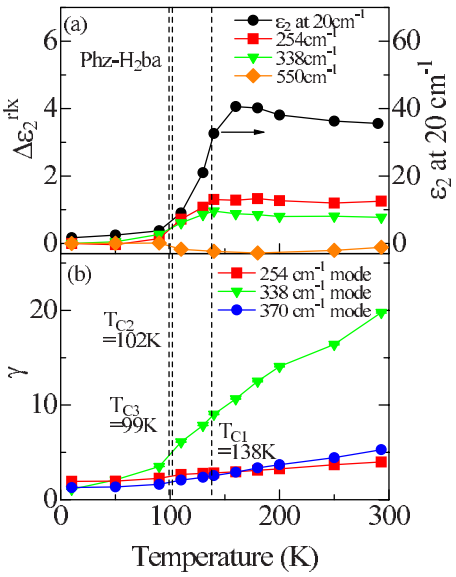

FIG. 9. (Color online) (a) T dependence of $\Delta\epsilon_2^{rlx}[=\epsilon_2^{rlx}(T)-\epsilon_2^{rlx}(10\ \mathrm{K})]$ at 254 cm^{-1} (squares), 338 cm^{-1} (triangles), and 550 cm^{-1} (diamonds) as well as ϵ_2 at 20 cm^{-1} (circles). (b) T dependence of γ for the 254 cm^{-1} mode (squares), the 338 cm^{-1} mode (triangles), and the 370 cm^{-1} mode (circles). The vertical dashed lines correspond to T_{C3}, T_{C2}, and T_{C1}, respectively, from left to right side.

frequency range. A similar low-frequency optical excitation is extensively observed in the conventional hydrogen-bonded ferroelectrics such as KDP. In KDP, a broad peak structure shows up around 70 cm^{-1} in ϵ_2 spectra in the course of the ferroelectric-to-paraelectric transition accompanying the melting of the proton ordering, when E is parallel to the hydrogen bond.[12,24,25] Although the origin of this optical excitation remains controversial, the most prevailing interpretation is the polarization relaxation mode coupled to the proton dynamics. In the present system, the polarity of the supramolecular chain originates from the intermolecular proton displacement. As mentioned in Sec. III A, the dynamical proton disorder is enhanced in the course of the melting of the periodic proton lattice at T_{C2} ($\sim T_{C3}$). Thus, the broad hump structure around 20 cm^{-1} may be attributed to the polarization relaxation mode coupled to the intermolecular dynamical proton displacement.

To see the coupling between the polarization relaxation mode and the molecular skeleton dynamics, we show the $E\|a$ ϵ_2 spectra in the wide frequency range of 0–5000 cm^{-1} in Fig. 8. At 10 K, many sharp peak structures originating from the librational/translational modes or the in-plane intramolecular vibrational modes are identified in the wide frequency range of 30–1700 cm^{-1}. At high temperatures, the polarization relaxation mode has a long tail extending up to 400 cm^{-1}, as exemplified as the shaded area in Fig. 8. It is evident that a few peak structures, for example, at 167 and 338 cm^{-1} (marked with open and closed triangles, respectively) are dramatically blurred, when going from 10 K to room temperature. Specifically, the prominent peak at 338 cm^{-1} originating from the C-O bending mode coupled to the C-Br stretching motion in H_2ba moiety is no more discernible at 293 K. It shows an asymmetric spectral shape characteristic of the Fano-type resonance,[26] which implies the interaction with the underlying broad continuum originating from the polarization relaxation mode. To quantitatively estimate the correlation between the mode broadening and the evolution of the polarization relaxation mode, we fitted the 338 cm^{-1} mode by the Fano formula[27]

$$\epsilon_2(\omega) = S\left\{\frac{[q+(\omega-\omega_0)/\gamma]^2}{1+(\omega-\omega_0)^2/\gamma^2}-1\right\}+\epsilon_2^{rlx}. \quad (1)$$

Here, S is the oscillator strength, γ the damping rate, q the Fano asymmetric parameter, ω_0 the peak frequency, and ϵ_2^{rlx} the contribution from the tail of the relaxation mode at ω_0. For comparison, we have also fitted the peak at 254, 370, and 550 cm^{-1}, which are assigned to the ring bending mode for Phz, the C=O bending mode coupled to the C-C stretching and C-O bending motion for H_2ba, and the C-Br stretching mode coupled to the ring bending motion, C-O bending motion and C=O bending motion for H_2ba moiety, respectively.[17,18] We identified the T dependence of the tail of the polarization relaxation mode at ω_0 by defining $\Delta\epsilon_2^{rlx}=\epsilon_2^{rlx}(T)-\epsilon_2^{rlx}(10\ \mathrm{K})$. In Fig. 9(a), we plotted $\Delta\epsilon_2^{rlx}$ at 254, 338, and 550 cm^{-1} as a function of T. We also plotted the T dependence of ϵ_2 at 20 cm^{-1} as a measure of the intensity of the polarization relaxation mode. As going from 10 K to higher temperatures, $\Delta\epsilon_2^{rlx}$ at 254 and 338 cm^{-1} is enhanced especially above T_{C2} ($\sim T_{C3}$), which is qualitatively consistent with the T dependence of ϵ_2 at 20 cm^{-1}. This suggests that the tail of the polarization relaxation mode subsists up to a frequency as high as 338 cm^{-1}. At 550 cm^{-1}, by contrast, $\Delta\epsilon_2^{rlx}$ remains to be almost T independent and hence the contribution from the tail of the polarization relaxation mode is thought to be negligible. In Fig. 9(b), we show the T dependence of γ for the 338 cm^{-1} mode as well as that

for the 370 and 254 cm^{-1} modes. The γ value for the 254 and 370 cm^{-1} modes show moderate T dependence. In contrast, the γ value for the 338 cm^{-1} mode steeply increases as T exceeds T_{C2} ($\sim T_{C3}$). These results suggest that the 338 cm^{-1} mode is selectively blurred and is amalgamated into the polarization relaxation mode above T_{C2} ($\sim T_{C3}$). As mentioned previously, the 338 cm^{-1} mode predominantly originates from the in-plane C-O bending motion in H_2ba moiety and hence may be particularly sensitive to the oxygen atom dynamics coplanar to the π-molecular plane. From these results, it is anticipated that the fluctuation of the in-plane π-molecular skeleton structure, specifically that of the oxygen atom, is anomalously enhanced and strongly coupled to the polarization fluctuation along the supramolecular chain; this occurs concomitantly with the enhancement of the dynamical proton disorder in the course of the melting of the periodic proton lattice. Such a strong correlation between the polarization fluctuation along the supramolecular chain and the in-plane π-molecular skeleton dynamics is distinct from the molecular skeleton dynamics along the π-molecular stacking direction ($\|b$); the intramolecular skeleton dynamics is barely coupled to the polarization fluctuation as described in Sec. III B.

Such a site-specific fluctuation of the proton π-molecular skeleton structure in the present system should be compared with the molecular skeleton dynamics of the proton order-disorder type organic ferroelectrics. The prototypical example is the cocrystal of 5,5′-dimethyl-2,2′-bipyridine (55DMBP) and iodanilic acid (H_2ia) in which the 55DMBP (base) and H_2ia (acid) moiety forms a supramolecular chain via the intermolecular bifurcated hydrogen bond with the proton shared by two oxygen atoms of H_2ia moiety and one nitrogen atom of 55DMBP moiety.[28] Recently, we have revealed that the proton delocalization in such a bifurcated hydrogen bond induces the anomalously large dynamical disorder in the π-molecular skeleton structure and almost all of the vibrational mode below 500 cm^{-1} disappears at the ferroelectric-to-paraelectric transition accompanying the melting of proton order.[29,30] In the presently investigated system, by contrast, the proton is almost confined in the linear O···N hydrogen bond since the carbonyl oxygen atom of H_2ba moiety least constitutes the hydrogen bond due to the long distance from the nitrogen atom of Phz moiety.[7,8] In such a linear hydrogen bond, the molecular structure shows a minimal coupling to the proton dynamics as compared with the bifurcated hydrogen-bond inherent in the 55DMBP-H_2ia. For example, the C=O bending motion is least coupled to the proton fluctuation as previously exemplified. In addition, the dynamical disorder of the proton is less prominent in the present system while the proton is broadly distributed at the center of the bifurcated hydrogen bond in the 55DMBP-H_2ia. Thus, the plausible origin for the site-selective nature of the π-molecular skeleton fluctuation may be the spatial confinement of the proton in the linear intermolecular hydrogen bond. From these results, it is anticipated that the geometrical configuration of the intermolecular hydrogen bond is an essential factor to control the dynamical disorder of the π-molecular skeleton structure coupled to the polarization fluctuation in these proton π-molecular skeleton coupled ferroelectrics.

IV. CONCLUSION

We have investigated the THz/infrared spectra for the proton-displacive organic ferroelectrics, cocrystal of phenazine with the 2,5-dihalo-3,6-dihydroxy-p-benzoquinones with the focus on the proton-mediated polarization π-molecular skeleton coupled dynamics. The soft phonon mode associated with the ferroelectric molecular displacement is identified around T_{C1} in the imaginary part of dielectric spectra (ϵ_2), when the electric field of the light (E) is parallel to the spontaneous polarization, that is, the π-molecular stacking direction (b axis). The soft phonon mode is least coupled to the intramolecular vibration mode and hence the polarization fluctuation along the π-molecular stacking direction is almost decoupled from the intramolecular skeleton dynamics. When E is parallel to the supramolecular chain (a axis), the polarization relaxation mode coupled to the proton dynamics can be identified in the course of the melting of the periodic proton lattice in ϵ_2 spectra. A few vibrational modes as represented by the C-O bending mode are blurred and amalgamated into the polarization relaxation mode. This suggests that the large fluctuation of the in-plane molecular skeleton structure, especially that of the oxygen atom, is induced by the dynamical proton disorder and strongly coupled to the polarization fluctuation along the supramolecular chain. From the comparison with the molecular skeleton dynamics in another class of order-disorder type ferroelectrics with the bifurcated intermolecular hydrogen bond, it is anticipated that the geometrical configuration of the intermolecular hydrogen bond to confine the proton motion is one of the essential factors to control the fluctuation of the π-molecular skeleton structures in these organic ferroelectrics.

ACKNOWLEDGMENTS

The authors wish to thank R. Kumai for fruitful discussions. This work was supported by Grants-in-Aid (Grants No.16740192, No. 17340104, No. 15104006, and No. 20110003) from JPSJ and MEXT, Japan.

[1] G. J. Goldsmith and J. G. White, J. Chem. Phys. **31**, 1175 (1959).
[2] R. G. Kepler and R. A. Anderson, Adv. Phys. **41**, 1 (1992).
[3] S. Horiuchi and Y. Tokura, Nature Mater. **7**, 357 (2008).
[4] S. Horiuchi, R. Kumai, and Y. Tokura, Chem. Commun. (Cambridge) (2007), 2321 .
[5] A. L. Solomon, Phys. Rev. **104**, 1191 (1956).
[6] S. Horiuchi, F. Ishii, R. Kumai, Y. Okimoto, H. Tachibana, N. Nagaosa, and Y. Tokura, Nature Mater. **4**, 163 (2005).
[7] R. Kumai, S. Horiuchi, H. Sagayama, T. H. Arima, M. Watanabe,

Y. Noda, and Y. Tokura, J. Am. Chem. Soc. **129**, 12920 (2007).
[8] S. Horiuchi, R. Kumai, and Y. Tokura, J. Mater. Chem. **19**, 4421 (2009).
[9] M. E. Lines and A. M. Glass, *Principles and Applications of Ferroelectrics and Related Materials* (Oxford University Press, New York, 1977).
[10] K. Saito, M. Amano, Y. Yamamura, T. Tojo, and T. Atake, J. Phys. Soc. Jpn. **75**, 033601 (2006).
[11] T. Asaji, T. J. Seliger, V. Zagar, M. Sekiguchi, J. Watanabe, K. Gotoh, H. Ishida, S. Vrtnik, and J. Dolinsek, J. Phys.: Condens. Matter **19**, 226203 (2007).
[12] P. Simon, F. Gervais, and E. Courtens, Phys. Rev. B **37**, 1969 (1988).
[13] S. Shin, Y. Tezuka, S. Saito, Y. Chiba, and M. Ishigame, J. Phys. Soc. Jpn. **63**, 2612 (1994).
[14] Y. Tominaga, H. Urabe, and M. Tokunaga, Solid State Commun. **48**, 265 (1983).
[15] Y. Moritomo, Y. Tokura, H. Takahashi, and N. Mori, Phys. Rev. Lett. **67**, 2041 (1991).
[16] N. Kida, Y. Ikebe, Y. Takahashi, J. P. He, Y. Kaneko, Y. Yamasaki, R. Shimano, T. Arima, N. Nagaosa, and Y. Tokura, Phys. Rev. B **78**, 104414 (2008).
[17] I. Bandyopadhyay and S. Manogaran, J. Mol. Struct.: THEOCHEM **507**, 217 (2000).
[18] A. Pawlukojc, G. Bator, L. Sobczyk, E. Grech, and J. Nowicka-Scheibe, J. Phys. Org. Chem. **16**, 709 (2003).
[19] F. Ishii, N. Nagaosa, Y. Tokura, and K. Terakura, Phys. Rev. B **73**, 212105 (2006).
[20] We could not measure the dielectric spectra below 30 cm^{-1} above 160 K with the transmission geometry of the THz-time-domain spectroscopy since the transmittance is too small to be measured. This is perhaps because the spectral weight in this frequency range is fairly large due to the evolution of the low-frequency optical excitation.
[21] J. F. Scott, Rev. Mod. Phys. **46**, 83 (1974).
[22] The data below 20 cm^{-1} is derived by the Kramers-Kronig analysis assuming the constant reflectivity.
[23] The possible explanation for this discrepancy may be the presence of the much lower frequency optical excitation such as the domain-wall dynamics. The domain-wall excitation is generally observed in the sub-GHz frequency range and often dominates the dielectric property in the audio-frequency range in a variety of the ferroelectrics. Such a low-frequency excitation cannot be captured in the present study and is an issue for the future.
[24] B. Wyncke and F. Brehat, J. Phys. C **19**, 2649 (1986).
[25] Y. Takagi and T. Shigenari, J. Phys. Soc. Jpn. **39**, 440 (1975).
[26] U. Fano, Phys. Rev. **124**, 1866 (1961).
[27] L. C. Davis and L. A. Feldkamp, Phys. Rev. B **15**, 2961 (1977).
[28] S. Horiuchi, R. Kumai, and Y. Tokura, Angew. Chem., Int. Ed. **46**, 3497 (2007).
[29] J. Fujioka, S. Horiuchi, F. Kagawa, and Y. Tokura, Phys. Rev. Lett. **102**, 197601 (2009).
[30] R. Kumai, S. Horiuchi, Y. Okimoto, and Y. Tokura, J. Chem. Phys. **125**, 084715 (2006).